Extrapolation Techniques for Very Low Cycle Fatigue Behavior of a Ni-base Superalloy

Brian R. Daubenspeck
e-mail: daubenspeck@knights.ucf.edu

Ali P. Gordon
e-mail: apgordon@mail.ucf.edu

Department of Mechanical, Materials, and Aerospace Engineering,
University of Central Florida,
Orlando, FL 32816-2450

A combination of extrapolation and estimation techniques from both prior and current studies has been explored with the goal of developing a method to accurately characterize high-stress amplitude low cycle fatigue of a material commonly used in gas turbine blades with the absence of such data. This paper describes innovative methods used to predict high-temperature fatigue of IN738LC, a dual-phase Ni-base superalloy. Three sets of experimental data at different temperatures are used to evaluate and examine the validity of extrapolation methods such as anchor points and hysteresis energy trends. High-stress amplitude data points approaching the ultimate strength of the material were added to pre-existing base data with limited plastic strain to achieve a full-range data set that could be used to test the legitimacy of the different prediction methods. Each method is evaluated at a number of temperatures. [DOI: 10.1115/1.4003602]

Keywords: very low cycle fatigue, IN738, high-temperature materials, Ni-base superalloy

1 Introduction

Accurate fatigue data are essential for the design of contemporary gas turbines under not only working loads but accidental and manufacturing loads also having a cyclic nature. Components in these devices are subjected to combinations of high temperature and mechanical cycling. A broad range of fatigue data increases this accuracy by providing insight to cyclic plastic strain. In most cases, there is a sufficient amount of high cycle fatigue (HCF) and relatively low-stress low cycle fatigue (LCF) data to ensure reliability within the common loading cycles. Characteristically, low cycle fatigue data are obtained via additional mechanical testing, which can be tedious and expensive [1,2]. Acquiring the LCF data from a pre-existing set of data would be of utmost efficiency. A strain-based fatigue curve consists of two linear sets of data to which a curve is fit: elastic strain data, which are always plentiful, and plastic strain data. The two sets of strain data, elastic and plastic, are used to form the lines of Basquin's equation and the Coffin–Manson equation, respectively. The equations of the lines are obtained through the intercepts, at $N_i=0.5$, and slopes derived from the linear regression process, i.e., Basquin's equation,

$$\varepsilon_{\mathrm{el},a} = \frac{\sigma_f'}{E}(2N_i)^b \tag{1}$$

and the Coffin–Manson equation

$$\varepsilon_{\mathrm{pl},a} = \varepsilon_f'(2N_i)^c \tag{2}$$

where $\varepsilon_{\mathrm{el},a}$ and $\varepsilon_{\mathrm{pl},a}$ are the elastic and plastic strain amplitudes, σ_f' is the fatigue strength coefficient, E is Young's modulus, b is the fatigue strength exponent, ε_f' is the strain ductility coefficient, c is the strain ductility exponent, and N_i is the cycle to initiation. The summation of these equations on a log-log plot is known as the total strain-life equation

$$\frac{\Delta\varepsilon_t}{2} = \frac{\sigma_f'}{E}(2N_i)^b + \varepsilon_f'(2N_i)^c \tag{3}$$

A cyclic strain-life plot, containing typical LCF test data, is presented in Fig. 1; in this case, all data are below the transition life N_t defined by $\Delta\varepsilon_{\mathrm{pl}}=\Delta\varepsilon_{\mathrm{el}}$. Iterative regression models can be utilized to optimize the strain-life fatigue constants. For Basquin's equation,

$$b = \frac{n\sum_{i=1}^{n}\log N_i \log \varepsilon_i^{\mathrm{el}} - \sum_{i=1}^{n}\log N_i \sum_{i=1}^{n}\log \varepsilon_i^{\mathrm{el}}}{n\sum_{i=1}^{n}\log(N_i^2) - \left(\sum_{i=1}^{n}\log N_i\right)^2} \tag{4}$$

$$\varepsilon^* = \frac{\sum_{i=1}^{n}\log \varepsilon_i^{\mathrm{el}} - b\sum_{i=1}^{n}\log N_i}{n} \tag{5}$$

$$\frac{\sigma_f'}{E} = 10^{\varepsilon^*}0.5^b \tag{6}$$

and the Coffin–Manson equation,

$$c = \frac{n\sum_{i=1}^{n}\log N_i \log \varepsilon_i^{\mathrm{pl}} - \sum_{i=1}^{n}\log N_i \sum_{i=1}^{n}\log \varepsilon_i^{\mathrm{pl}}}{n\sum_{i=1}^{n}\log(N_i^2) - \left(\sum_{i=1}^{n}\log N_i\right)^2} \tag{7}$$

$$\varepsilon^* = \frac{\sum_{i=1}^{n}\log \varepsilon_i^{\mathrm{pl}} - c\sum_{i=1}^{n}\log N_i}{n} \tag{8}$$

$$\varepsilon_f' = 10^{\varepsilon^*}0.5^c \tag{9}$$

where N is the cycle to initiation, n is the number of data being exploited, $\varepsilon^{\mathrm{el}}$ is the elastic strain amplitude, and $\varepsilon^{\mathrm{pl}}$ is the plastic strain amplitude, in which the strains can be normalized by ε_o.

Contributed by the Materials Division of ASME for publication in the JOURNAL OF ENGINEERING MATERIALS AND TECHNOLOGY. Manuscript received May 20, 2010; final manuscript received January 18, 2011; published online March 23, 2011. Assoc. Editor: Thomas Siegmund.

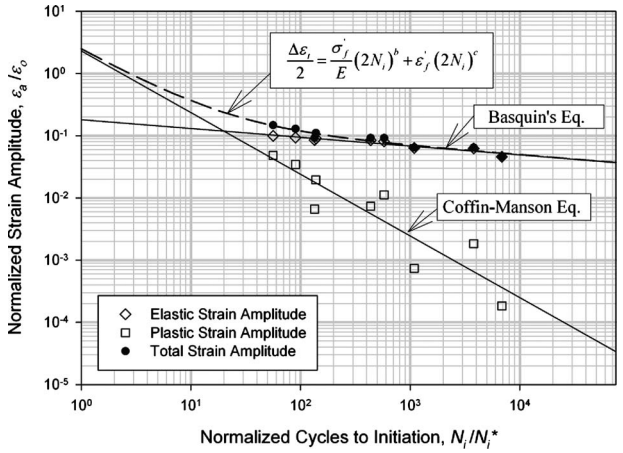

Fig. 1 Typical LCF test data for a Ni-base superalloy

Performing a linear regression to estimate lives in the region of N_t with a set of points where $\Delta\varepsilon_{pl} \ll \Delta\varepsilon_{el}$ is not practical. Test data with cycles to failure from 1 to 100 have hysteresis loops dominated by the plastic strain response of the material; however, as previously stated, cyclic testing is usually conducted for necessary stress relevant to service conditions where $\Delta\sigma < 2\sigma_y$. These stress ranges, although sometimes considered as low cycle fatigue, will have inadequate plastic strain with cycles to failure above 10^4. It should be noted that fatigue with cycles to failure around 100 and below is termed very low cycle fatigue (VLCF) or extremely low cycle fatigue (ELCF) and, in most cases, exhibits uncharacteristic trends [3].

The goal of the current research is to explore existing techniques that are used to extrapolate LCF data to high-stress (or strain) amplitudes using pre-existing data sets with inadequate cyclic plastic strain and to design a method that can accurately predict high-stress LCF of high-temperature IN738LC. The LCF data at high-stress amplitudes can be crucial when choosing between different materials [4], estimating the life expectancy of an element that has just received an accidental overload, or predicting the likelihood of cracking during cyclic forming processes. Although approximation techniques are available to characterize LCF data, few have been tested with Ni-base superalloys at elevated temperatures. Eminent methods of approximation such as Manson's universal slopes [5,6], Manson's four point [5], and the modified four point by Ong [7], originally designed for room temperature steel alloys, have little correlation with the high-temperature LCF data of IN738LC. These approximation methods are generally calculated based on historical observations from phenomenological behavior and/or functions of tensile test properties [1,2]. Less broadly used methods that exist for LCF predictions of Ni-base superalloys are only useful for estimating boundaries and cannot accurately characterize LCF. Considering that there are several uses of Ni-base superalloys, in this case gas turbine components, the development of a technique to either extrapolate or estimate high-stress amplitude fatigue within these alloys for wide-ranging temperatures would be an extraordinary contribution that can help lower the costs of inspection, repair, and replacement of certain engine components.

2 Test Material

Gas turbine engines are designed to operate at a maximum temperature between 1100°C and 1300°C, but due to coatings and cooling techniques, most experimental test data are needed in the range of 750–950°C [8]. In the hot gas path region, Ni-base superalloys are often employed due to their strength against creep and fatigue mechanisms of damage. For this study, Ni-base superalloy IN738LC (Inconel 738 low carbon) is used. These properties are attributed to a face-centered-cubic (fcc) γ matrix that is hardened by apt solutes and fine precipitates [9]. The precipitates, termed γ', strengthen the material by slowing down dislocations; this phase makes up 48% of the total volume. Along with the γ matrix and γ' phase, this multiphase alloy consists of $M_{23}C_6$, MC, and TiN [10]. The chemical compositions of IN738 and IN738LC are shown in Table 1. The principal distinction between IN738 and the slightly altered version, IN738LC, is the reduction of carbon and zirconium contents within IN738LC. These modifications to IN738LC improve the castability among larger section sizes and marginally improve mechanical properties and corrosion resistance [11]. Generally, both materials are in the form of as-cast or precipitation-hardened investment castings. Young's modulus, yield strength, ultimate tensile strength, and other imperative properties of IN738LC as functions of temperature are documented in both Table 2 and Fig. 2; the material used in this research boasts a medium microstructure with a precipitate size of approximately 450 nm. Although the overall strength of the material decreases with increased temperature, the mechanical properties of IN738LC remain superior in high-temperature conditions. The increase in yield strength for the medium, coarse, and duplex microstructures with temperatures following 750°C is also noteworthy. Many Ni-based superalloys have a similar chemical makeup and are used in parallel with IN738LC in turbine engine design [12].

Table 1 Chemical composition of IN738LC (wt %) [10,11]

Alloy	Ni	Cr	Co	Al	Ti	W	Mo	Ta	Nb	C	Zr	B
IN738LC	Bal	16	8.5	3.4	3.4	2.6	1.75	1.75	0.9	0.11	0.07	0.01
IN738	Bal	16	8.5	3.5	3.5	2.6	1.8	1.8	0.9	0.16	0.08	0.01

Table 2 Mechanical properties on IN738LC from literature [1,9,16,18]

	Temperature T (°C)		
Mechanical property	24 (RT)	750	850
Elastic modulus E (GPa)	170–190 [1,9]	123–160 [1,9,16]	126–150 [1,9,16]
Poisson's ratio ν	0.29 [17]	N/A	N/A
0.2% yield strength σ_y (MPa)	710 [9]	580 [9]	600 [9]
Ultimate tensile strength σ_{UTS} (MPa)	850 [1,9]	790–825 [1,9]	675–740 [1,9]
Fracture strain ε_f (%)	5.5–11.5 [1,9]	8.6–11.5 [1,9]	10.8–13.0 [1,9]
Fracture toughness K_C (MPa $m^{1/2}$)	72 [18]	33 [18]	43 [18]

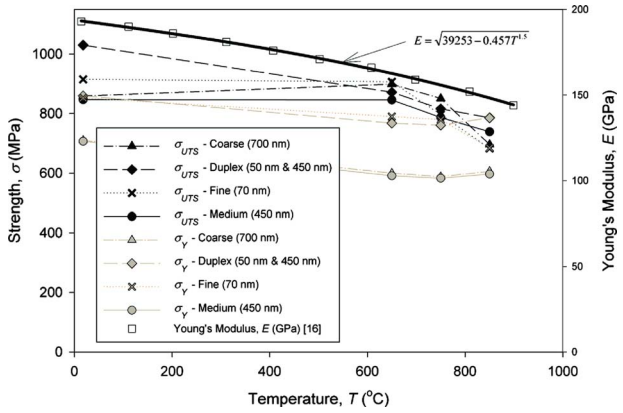

Fig. 2 Material properties of IN738LC as functions of temperature [9,16]

The data used in this research include tensile tests and fully reversed cyclic tests at 24°C, 750°C, and 850°C; these temperatures are commonly realized in turbine blades. Conventionally, cast IN738LC is being used as opposed to directionally solidified (DS) or single crystal (SC) alloys because of fiscal incentives to fully utilize the less expensive cast alloys. Both DS and SC Ni-base superalloys provide for advanced fatigue and creep properties and are often used in turbine blade construction, but are not always cost effective with a high ratio of price to performance [13].

The typical processing conditions for specimens machined from cast slabs of IN738LC can vary. The IN738LC material is generally hot isostatically pressed (HIPd) for between 1 h and 4 h under 75–125 MPa at 1100–1300°C and then cooled slowly at a controlled rate while appropriately depressurizing [9]. After maintaining the slab at around 1100°C for several more hours, the material is gas quenched to room temperature in less than 5 min. Precipitation hardening is then generally achieved via heating, cooling, and thermal shocking techniques. The specimen design used for mechanical testing in this study, illustrated in Fig. 3, is in conformance with ASTM standard E606-04 [14]. A 0.75 in. gauge length is employed with a 0.25 in. diameter and an axially polished 0.2 μm surface finish.

3 Experimental Methods

The strain-controlled fatigue data in this study, administered to consolidate the $\varepsilon-N$ behavior of the material, can be categorized into three subgroups: (1) "baseline" data where $\Delta\varepsilon_{pl} < \Delta\varepsilon_{el}$, (2) "ELCF" data common with accidental overload situations, i.e., $\Delta\varepsilon_{pl} \approx \Delta\varepsilon_{el}$, and (3) tensile data, which along with baseline data, are used to establish extrapolation methods. The procedure used to test the extrapolation techniques begins by first making predictions of high-stress amplitude behavior using a base data set with limited plastic strain. The base data set used in this study is documented in Table 3. Several high-stress amplitude data tests, listed

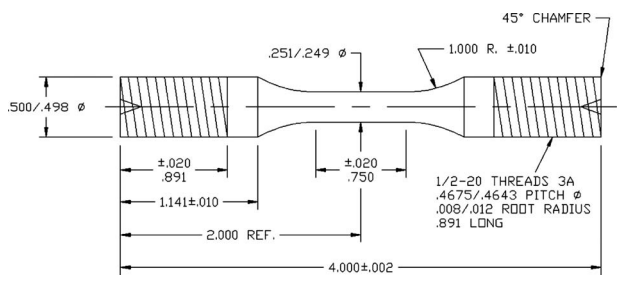

Fig. 3 Test specimen used in the current study (inches)

Table 3 LCF base data for IN738LC; strain rate for each case is 10^{-3} s^{-1}

Temperature T (°C)	Norm. strain range, $\Delta\varepsilon/\varepsilon_o$	Quantity
24	0.147	1
24	0.184	1
750	0.092	1
750	0.129	2
750	0.184	3
850	0.074	2
850	0.092	2
850	0.110	2
850	0.129	1
850	0.147	1
850	0.184	8

in Table 4, with ample plastic strain were then incorporated to form an archetypal strain-life curve. The experimental and predicted cycles to initiation are then plotted against a 45 deg line for correlation conception. The Pearson product R^2 is used to evaluate the less conspicuous high-temperature extrapolation correlations.

For proprietary intentions, the predominant LCF data found in this study have been normalized via room temperature references. It should be noted, however, that IN738LC fatigue data are widely available and un-normalized in several sources. Related strain-life data gathered from a number of these sources, plotted with cycles to failure, are shown in Fig. 4. Although similar trends are observed in these LCF data, disparate strain rates and initiation/failure criteria prevent a reliable amalgamation with data utilized in this study. Considering that every symbol could not be added to the legend, each set of data in the following figure has a particular testing temperature and strain rate indicated with a specific color and shape. Total, elastic, and plastic strains, where available, are symbolized by empty, semifilled top, and semifilled bottom icons, respectively. The distinctions between the versions of IN738LC

Table 4 LCF augmented data for IN738LC; strain rate for each case is 10^{-3} s^{-1}

Temperature T (°C)	Norm. strain range, $\Delta\varepsilon/\varepsilon_o$	Specimen ID
24	0.221	D912-20
24	0.257	D912-19
24	0.294	D912-25
750	0.221	D912-6
750	0.257	D912-14
750	0.294	D912–8
850	0.221	D912-16
850	0.257	D912-15
850	0.294	D912-11

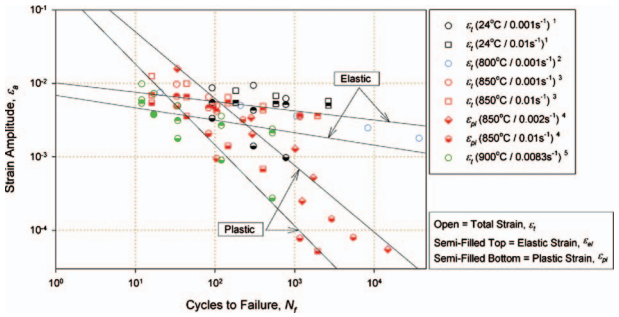

Fig. 4 Un-normalized strain-life data gathered from various sources [10,19–22]

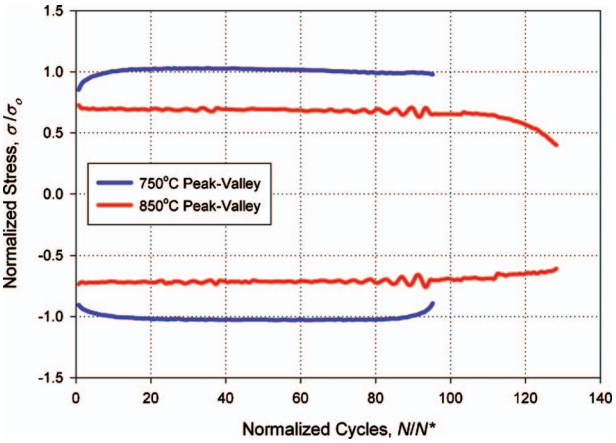

Fig. 5 Stress histories for specimens D912-14 and D912-15 at 750°C and 850°C, respectively

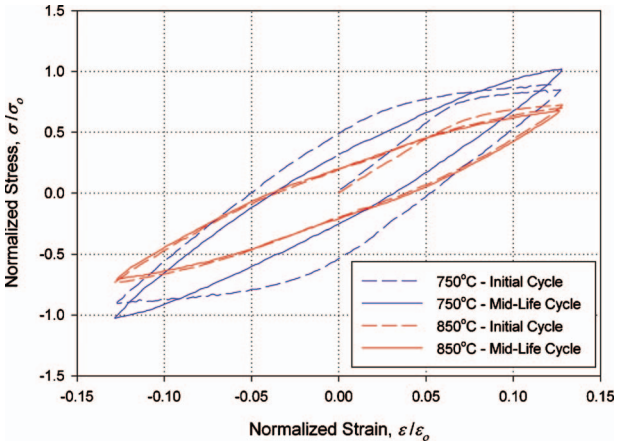

Fig. 6 Hysteresis loops for specimens D912-14 and D912-15 at 750°C and 850°C, respectively

used in these data are discussed in the respective papers. Only a single test at 900°C, within all of the data, exhibits plastically dominant VLCF behavior.

The main focus of this research, however, to exemplify trends and to formulate extrapolation methods is not affected through these normalizing measures. Values denoting stress and strain are normalized by room temperature references, i.e., σ/σ_o and $\varepsilon/\varepsilon_o$, respectively. Cycles to initiation N_i have been divided through by an arbitrary constant N_i^*.

The testing was carried out on an MTS load frame assembly equipped with both a thermocouple and an extensometer for temperature and strain control, respectively. The isothermal strain-controlled LCF data collected in this research are fully reversed with a strain rate of 10^{-3} s^{-1} and comply with ASTM standards. A 5% load drop was assumed in this research to signify crack initiation.

4 Experimental Results

A complete collection of the raw augmented data was accessible for this study, and as such, the results of these tests will be discussed. Although the base data used in the research were assembled from past research, comparisons among the elastic moduli and yield strengths at 750°C and 850°C deemed them compatible [1]. From the augmented tests, stress versus cycles (stress histories) and cyclic stress-strain curves (hysteresis loops) were exploited to determine strain hardening or softening effects, crack initiations, and stabilization periods in conjunction with associated stress and strain ranges.

By evaluating initial and stabilized stress ranges from both the stress histories and hysteresis loops, strain hardening was shown to occur at 24°C and 750°C while strain softening was observed at 850°C. These assessments are in agreement with previous studies of IN738LC. Strain hardening, at 750°C, is depicted in both Figs. 5 and 6; similar hardening effects intensified with increased strain ranges for both 24°C and 750°C. However, strain softening at 850°C diminished as the strain ranges increased. It should be noted that significantly less strain hardening occurred at 24°C for the two elevated strain range tests when compared with equivalent strain ranges at 750°C.

From Fig. 5, the cyclic stress history at 750°C reveals that stabilization occurred by normalized cycle 20; a 5% load drop from the stabilized stress range, signifying crack initiation, transpired around normalized cycle 90. While deviations in the strain range cannot be directly measured from these plots alone, it is evident whether there was a lack of control during testing. The coarse testing displayed in Fig. 5 at 850°C realized a maximum deviation of 13.2% from the strain range. Problematic strain control was more prevalent in the high-temperature testing; however, the majority of tests were within 3% of their designated strain range as per ASTM standard.

5 Extrapolation Techniques

5.1 Model 1—MAP. An anchor point is a monotonic test data point superimposed into a pre-existing data set. This technique allows for an enhanced qualitative fit of the strain-based curves outside of the plastically inferior base data. The technique used to incorporate the anchor point is analogous to the inclusion of other data: treat the point as a fatigue data point compromised of plastic and elastic strains at one-half cycles during the linear regression process [1,2]. The plastic strain is approximated as the elongation at failure ε_f of the monotonic tensile test while the elastic strain is calculated by dividing the failure stress σ_f by the elastic modulus E, i.e.,

$$\varepsilon_{f,\mathrm{pl}} = \varepsilon_f \tag{10}$$

$$\varepsilon_{f,\mathrm{el}} = \frac{\sigma_f}{E} \tag{11}$$

As a rule, the elongation at failure, corresponding to ductility, increases with temperature. The elevated measure of plasticity and the customary availability of monotonic tensile tests contribute to the appeal of this well-known method. Plastic deformation obtained through the tensile test is comparable to that which would be observed via a high-strain fatigue test. In this research, strain hardening and softening effects are achieved through multiple cycles of strain-controlled fatigue tests; consequently, these effects are neither witnessed nor integrated into the anchor point method.

This novel approach was established to optimally adjust the anchor point for extrapolation and ascertain whether or not such an attunement could be resolved to enhance LCF predictions for increased temperatures. Research by Radonovich [1] confirmed that the basic anchor point significantly underestimates typical VLCF behavior of IN738LC; however, it is to be determined whether these trends of inaccuracy at high temperatures exhibit similarities. By utilizing the augmented data, scaling constants for both elastic and plastic strains of the anchor point will be investigated to quantify the error associated with the basic anchor point method at 750°C and 850°C. The optimal scaling factors of the two elevated temperatures are averaged to develop a single set of scales for the elastic and plastic portions of a high-temperature IN738LC anchor point. This set of scales is then used to adjust the

Table 5 Temperature dependence of anchor point scaling factors

Temperature T (°C)	Elastic factor C_{el}	Plastic factor C_{pl}
24	298	2.30
750*	241	4.35
850*	310	3.15
Average of HT* factors	275.5	3.75

basic anchor point components through multiplication for an improved extrapolation of high-strain data at increased temperatures. For Basquin's equation,

$$b = \frac{n\sum_{i=1}^{n} \log N_i \log C_{el}\varepsilon_i^{el} - \sum_{i=1}^{n} \log N_i \sum_{i=1}^{n} \log C_{el}\varepsilon_i^{el}}{n\sum_{i=1}^{n} \log(N_i^2) - \left(\sum_{i=1}^{n} \log N_i\right)^2} \tag{12}$$

$$\varepsilon^* = \frac{\sum_{i=1}^{n} \log C_{el}\varepsilon_i^{el} - b\sum_{i=1}^{n} \log N_i}{n} \tag{13}$$

$$\frac{\sigma_f'}{E} = 10^{\varepsilon^*} 0.5^b \tag{14}$$

and the Coffin–Manson equation,

$$c = \frac{n\sum_{i=1}^{n} \log N_i \log C_{pl}\varepsilon_i^{pl} - \sum_{i=1}^{n} \log N_i \sum_{i=1}^{n} \log C_{pl}\varepsilon_i^{pl}}{n\sum_{i=1}^{n} \log(N_i^2) - \left(\sum_{i=1}^{n} \log N_i\right)^2} \tag{15}$$

$$\varepsilon^* = \frac{\sum_{i=1}^{n} \log C_{pl}\varepsilon_i^{pl} - c\sum_{i=1}^{n} \log N_i}{n} \tag{16}$$

$$\varepsilon_f' = 10^{\varepsilon^*} 0.5^c \tag{17}$$

where

$$C_{el} = \begin{Bmatrix} 298.0 & \text{if RT tensile data} \\ 275.5 & \text{if HT tensile data} \\ 1.0 & \text{if base data} \end{Bmatrix},$$

$$C_{pl} = \begin{Bmatrix} 2.30 & \text{if RT tensile data} \\ 3.75 & \text{if HT tensile data} \\ 1.0 & \text{if base data} \end{Bmatrix}$$

Here, C_{el} and C_{pl} serve as piecewise fitting constants. The terms RT and HT refer to room temperature and high temperature, respectively.

The scaling factors for the high-temperature anchor point adjustments used in this method are shown in Table 5 along with a set of factors suitable for room temperature extrapolation. The average factors displayed incorporate the 750°C and 850°C modifications only and are not a function of the room temperature alteration. It should be noted again that this method implements the augmented data to formulate the extrapolation process and quantify errors associated with the basic anchor point. Using the augmented data in such a manner has not yet been attempted. The decrease in the multiplicative plastic factor for 850°C is due to strain softening effects and a decrease in overall strength of the material.

5.2 Model 2—WIP. Increased scatter within the plastic data is predominantly located at longer lives where elastic strain prevails, i.e., low-stress regions. By weighting the base data with cycles to initiation below 1000, an improved linear regression of the Coffin–Manson equation is possible. For Basquin's equation,

$$n' = n + \bar{n}$$

where $\bar{n}$ is the number of data points with $N \leq 1000$, i.e.,

$$b = \frac{n'\sum_{i=1}^{n'} A \log N_i \log \varepsilon_i^{el} - \sum_{i=1}^{n'} A \log N_i \sum_{i=1}^{n'} A \log \varepsilon_i^{el}}{n'\sum_{i=1}^{n'} A \log(N_i^2) - \left(\sum_{i=1}^{n'} A \log N_i\right)^2} \tag{18}$$

$$\varepsilon^* = \frac{\sum_{i=1}^{n'} A \log \varepsilon_i^{el} - b\sum_{i=1}^{n'} A \log N_i}{n'} \tag{19}$$

$$\frac{\sigma_f'}{E} = 10^{\varepsilon^*} 0.5^b \tag{20}$$

and the Coffin–Manson equation,

$$c = \frac{n'\sum_{i=1}^{n'} B \log N_i \log \varepsilon_i^{pl} - \sum_{i=1}^{n'} B \log N_i \sum_{i=1}^{n'} B \log \varepsilon_i^{pl}}{n'\sum_{i=1}^{n'} B \log(N_i^2) - \left(\sum_{i=1}^{n'} B \log N_i\right)^2} \tag{21}$$

$$\varepsilon^* = \frac{\sum_{i=1}^{n'} B \log \varepsilon_i^{pl} - c\sum_{i=1}^{n'} B \log N_i}{n'} \tag{22}$$

$$\varepsilon_f' = 10^{\varepsilon^*} 0.5^c \tag{23}$$

Here,

$$A = \begin{Bmatrix} 1.0 & \text{if } N > 1000 \\ 2.0 & \text{if } N \leq 1000 \end{Bmatrix}, \quad B = \begin{Bmatrix} 1.0 & \text{if } N > 1000 \\ 2.0 & \text{if } N \leq 1000 \end{Bmatrix}$$

The theory is that doubling the data with more copious amounts of plastic strain will fortify the linearity seen in these strain ranges and reduce the effects of scatter found at longer lives. A potential shortcoming with this innovative method is that Basquin's equation is additionally influenced by the weighting of elastic data associated with high plasticity. Considering that there are only two data points in the base data set for 24°C, neither of which have increased plastic strain; this method is only applicable for the 750°C and 850°C base data sets.

5.3 Model 3—Original Basquin's (OB) Equation Perpetuation. Attempting to extrapolate from plastically inferior data does not constitute grounds for adjusting ample elastic strain data. These elastic strain data are valid and may not need to be attuned with anchor points or weighting techniques; therefore, maintaining Basquin's equation from the original base data is proposed. The two preceding methods can be corrected to utilize this concept.

1. When employing either the anchor point or modified version via the scaling factors, simply do not include the elastic

failure strain during the linear regression of Basquin's equation; instead, use only the Coffin–Manson factors

$$C_{\text{pl}} = \begin{Bmatrix} 2.30 & \text{if RT tensile data} \\ 3.75 & \text{if HT tensile data} \\ 1.0 & \text{if base data} \end{Bmatrix}$$

In subsequent figures and graphs, this model will be displayed as model 3.1 (OBMAP).

2. In attempting to weight the plastically superior base data, only include the plastic data along with the cycles to initiation in the regression process; this will impede any alterations in the elastic data:

$$n' = n + \bar{n}, \quad B = \begin{Bmatrix} 1.0 & \text{if } N > 1000 \\ 2.0 & \text{if } N \leq 1000 \end{Bmatrix}$$

Such a technique will be denoted as model 3.2 (OBWIP).

For IN738LC, data above 1000 cycles exhibit decreased levels of plasticity, where $\Delta\varepsilon_{\text{pl}} \ll \Delta\varepsilon_{\text{el}}$.

5.4 Model 4—Plastic Hysteresis Energy Density Trends (HEP). Another quantitative facet of the cyclic stress-strain hysteresis loop is known as strain energy density. The total hysteresis energy density (u_t) is defined as the sum of the elastic (u_{el}) and plastic (u_{pl}) hysteresis energies, i.e.,

$$u_t = u_{\text{el}} + u_{\text{pl}} \tag{24}$$

Plastic strain energy density can be defined as the area within the hysteresis loop; furthermore, elastic strain energy density can be calculated by summing the two triangular regions flanked by the outer parameter of the hysteresis loop and the abscissa. Energetistic formulations can be devised to mathematically vindicate strain energy density,

$$u_{\text{el}} = \frac{\sigma_{\max}^2}{E} \tag{25}$$

$$u_{\text{pl}} = 2\int_{-\varepsilon_{\text{pl},a}}^{\varepsilon_{t,a}} \sigma(\varepsilon)d\varepsilon - \frac{\sigma_{\max}^2}{E} \tag{26}$$

While it has been habitually neglected in LCF lifetime prediction methods, hysteresis stress ($\Delta\sigma$) has proven to be a fundamental factor in the damage process. Recently, proposed hysteresis energy techniques incorporate this stress effectively. At increased cyclic stresses, as realized in LCF and VLCF applications, fatigue damage is primarily associated with plastic strain energy dissipation [15].

In this proposed method, the LCF energy density data of IN738LC, obtained from midlife hysteresis loops, are calculated in an attempt to identify the optimal ELCF prediction approach for the candidate material. The energy calculations obtained from hysteresis loops of the augmented data series are investigated to show whether plastic strain energy density can be solely computed from the midlife plastic strain and stress ranges, i.e., u_{pl} as a function of $\Delta\varepsilon_{\text{pl}}$ and $\Delta\sigma$. Additionally, accumulated hysteresis energy, defined as the product of the midlife stress range and plastic strain range, is calculated for each individual test in both the base and augmented data series. Such formulations are then plotted to reveal lifetime trends with varying energy densities. Although this method has been previously implemented for other Ni-base superalloys, tendencies within the LCF data of IN738LC are undeveloped.

6 Modeling Results

In this section, comparisons will be made between the models presented and the related archetypal representations created from the base and augmented data. The strain-life base data model, using strictly the base data, and the augmented data model, employing both the augmented and base data, were created through linear regression as described earlier. The energy-life models were created using tensile, base, and augmented data to realize the tendencies of each temperature. Table 6 displays the data sources employed into the models. For brevity, strain-life and energy-life data are plotted together; however, since strain and energy are not linear, data cannot be overlaid.

Table 6 Data sources for the individual models

Model	Tensile data	Base data	Augmented data
Base data model	X	✓	X
Augmented data model	X	✓	✓
Model 1—MAP	✓	✓	✓
Model 2—WIP	X	✓	X
Model 3.1—OBMAP	✓	✓	✓
Model 3.2—OBWIP	X	✓	X
Model 4—HEP	✓	✓	✓

The inclusion of room temperature data was necessary to understand LCF behavior of IN738LC beyond the elevated temperature region. Although only five data points exist at 24°C, execution of particular models proved functional. The modified anchor point (MAP) and OBMAP models, which made use of the augmented data in creating a MAP, were able to drastically improve upon the base data model; this perception is depicted in Fig. 7. The base data model severely deviates from the augmented data while the other three models clearly enhance extrapolation. Further analyses of the strain-life models will be presented later via life-life plots. Linear regression of the hysteresis energy data at 24°C, additionally displayed in Fig. 7, modeled the trend surprisingly well, considering the lack of data. It should be noted that the tensile data, modeled as $4\sigma_{\text{UTS}}\varepsilon_{f,\text{pl}}$, did not necessitate scaling and correlated well with the LCF data.

The first elevated temperature data to be modeled in this study were at 750°C. Recalling that the base data set at this temperature included six data points, the capabilities of this model are more consistent with the needs of designers based on ASTM standards. A comparison of the models used at this temperature is shown in Fig. 8. The MAP and OBMAP models, using the average scaling factors presented in Table 5, were able to successfully capture the augmented data. The other two formulated models, weighting of increased plasticity (WIP) base data and OBWIP, are nearly identical and extrapolate just below the base data model. When compared with the base data model, the MAP and OBMAP models are less conservative in the VLCF ranges. More conservative bounds are established through the WIP and OBWIP models.

Hysteresis energy for the 750°C data is presented in Fig. 8 as well; the slope of this regression fit is noticeably steeper than that

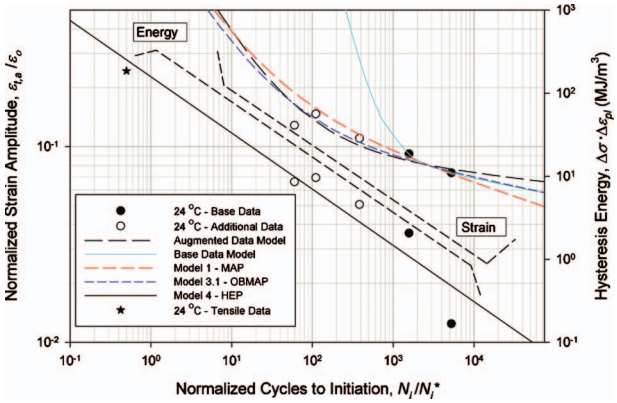

Fig. 7 Comparison of the strain-life models and hysteresis energy-life data regression at 24°C

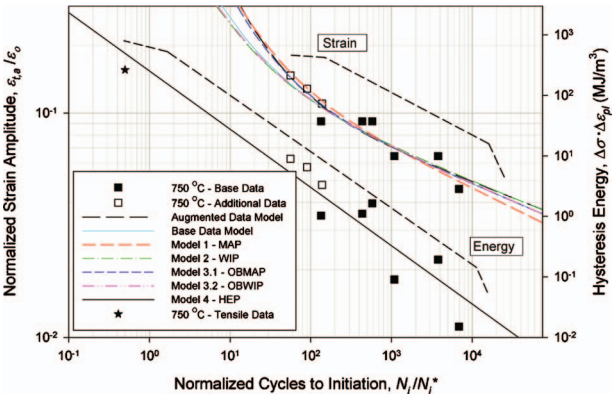

Fig. 8 Comparison of the strain-life models and hysteresis energy-life data regression at 750°C

of the energy at 24°C. Once again, the tensile data show a naturally strong correlation to the LCF data and are just below the least-squares regression line.

Analogous to the other two temperatures, the 850°C augmented data set included three increased strain range tests; however, an expanded base data set consisted of 16 data points. The models employed at this temperature are shown in Fig. 9. The augmented data model in this figure lies just beneath the base data model until around normalized cycle 10 because of the increased influence of the copious base data set. The interrelated models MAP-OBMAP and WIP-OBWIP seem to mostly differ at longer lives. All of the developed models at this temperature are less conservative than both the base data and augmented data strain-life models; however, the best model at this temperature is not evident thus far.

Linear regression of the hysteresis energy data at 850°C is also shown in Fig. 9. Very little scatter is observed in this case, and the tensile data demonstrate similar strong-correlation tendencies. The slope of this regression line is slightly less steep than the 750°C case.

A particular strain-life extrapolation method is not only judged on how well the augmented data were estimated but how effectively the base data were characterized via the estimation. The plots compiled in Fig. 10 allow for meticulous examination into the effect each method had on the groups of temperature dependent data.

As can be seen through the augmented data model, the augmented data at 24°C are quite scattered; however, two of these data are within a factor of 2 scatter band represented by the solid lines. The augmented data at 750°C and 850°C all fall within a

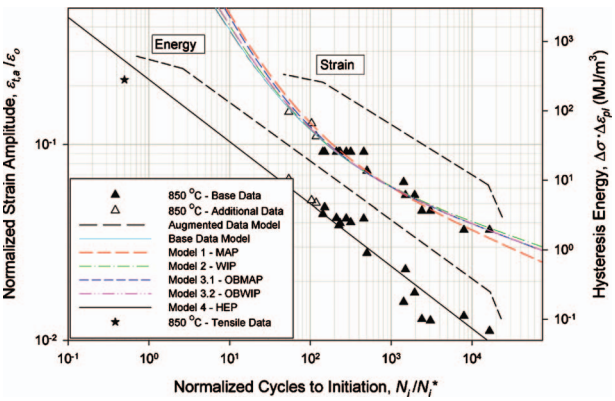

Fig. 9 Comparison of the strain-life models and hysteresis energy-life data regression at 850°C

factor of 1.5 scatter band represented by the dashed-dot-dot lines. Data tend to disperse as they reach greater lives in the base data set, indicating that this model may not perform as expected, i.e., the best overall fit.

The initial model implemented, MAP, better predicts the augmented data for 24°C as compared with the base data model. All but one of the room temperature data is inside a factor of 1.5 scatter band, suggesting a better overall fit from both the base and augmented data models. From the display, it can be seen that extrapolation to the 750°C augmented data has almost been perfected, even beyond that of the augmented data model. The base data predictions for this temperature, excluding one point, have also been improved. The augmented data predictions at 850°C have been negatively influenced; however, the base data estimations have been enhanced from both the augmented and base data models.

The WIP model, which was applicable to the 750°C and 850°C data sets, is assessed in Fig. 10. This model is nearly identical to that of the base data model and actually negatively affects the base data predictions for both temperatures. Augmented data estimations at 750°C are still within a factor of 1.5 scatter band; yet, without trumping the base data model, it remains unimposing. Conversely, at 850°C, extrapolation capacity is superior to all previous models. Pearson product (R^2) correlations presented later in this section validate these claims.

The OBMAP model solely employs an anchor point for the plastic Coffin–Manson equation. For the room temperature case, this model was able to better predict augmented data while only negatively affecting one of the base data points when compared with the MAP model. At 750°C, the OBMAP model, as compared with the MAP model, improved upon some of the base data approximations and slightly surpassed augmented data extrapolation. Conversely, when compared with the MAP model, 850°C augmented data approximations were improved, whereas some base data were negatively influenced.

The OBWIP model was only able to positively impact one of the base data at 750°C from the WIP model. At 850°C, a few more of the base data were able to be better approximated with this model when compared with the WIP model. Extrapolation abilities of this model are superior to those of the WIP model as well; therefore, this model provided the best extrapolation at 850°C while utilizing the least amount of data.

The prediction aptitude of the hysteresis energy trend model, without the inclusion of an anchor point, is shown lastly in Fig. 10. This method, as compared with the augmented strain-life data models, enhanced augmented extrapolation at 24°C and 850°C. Significant scatter exists in the base data predictions for all temperatures; however, the majority of augmented data are inside a factor of 1.5 scatter band. Notice that in all strain-life models, similar strain amplitudes are horizontally aligned; alternatively, this trend is not observed in the energy model. The ability of this model to factor multiple variables into the lifetime predictions enhances its flexibility. A quantitative analysis (R^2) for the high-temperature extrapolation abilities of the individual models is displayed in Table 7.

Of the developed methods of approximation, the MAP and OBMAP models were able to provide the greatest extrapolation improvement over the base data and augmented data models at 750°C. As for the WIP and OBWIP models, both may be considered as bounding estimates for the presented data at 750°C; however, at 850°C, these models surpassed the extrapolation abilities of the augmented and base data models. Using similar data, the HEP model improved augmented life estimation at 850°C over the strain-life augmented data model. The HEP model was also shown to moderately characterize fatigue and improve upon augmented data predictions at 24°C.

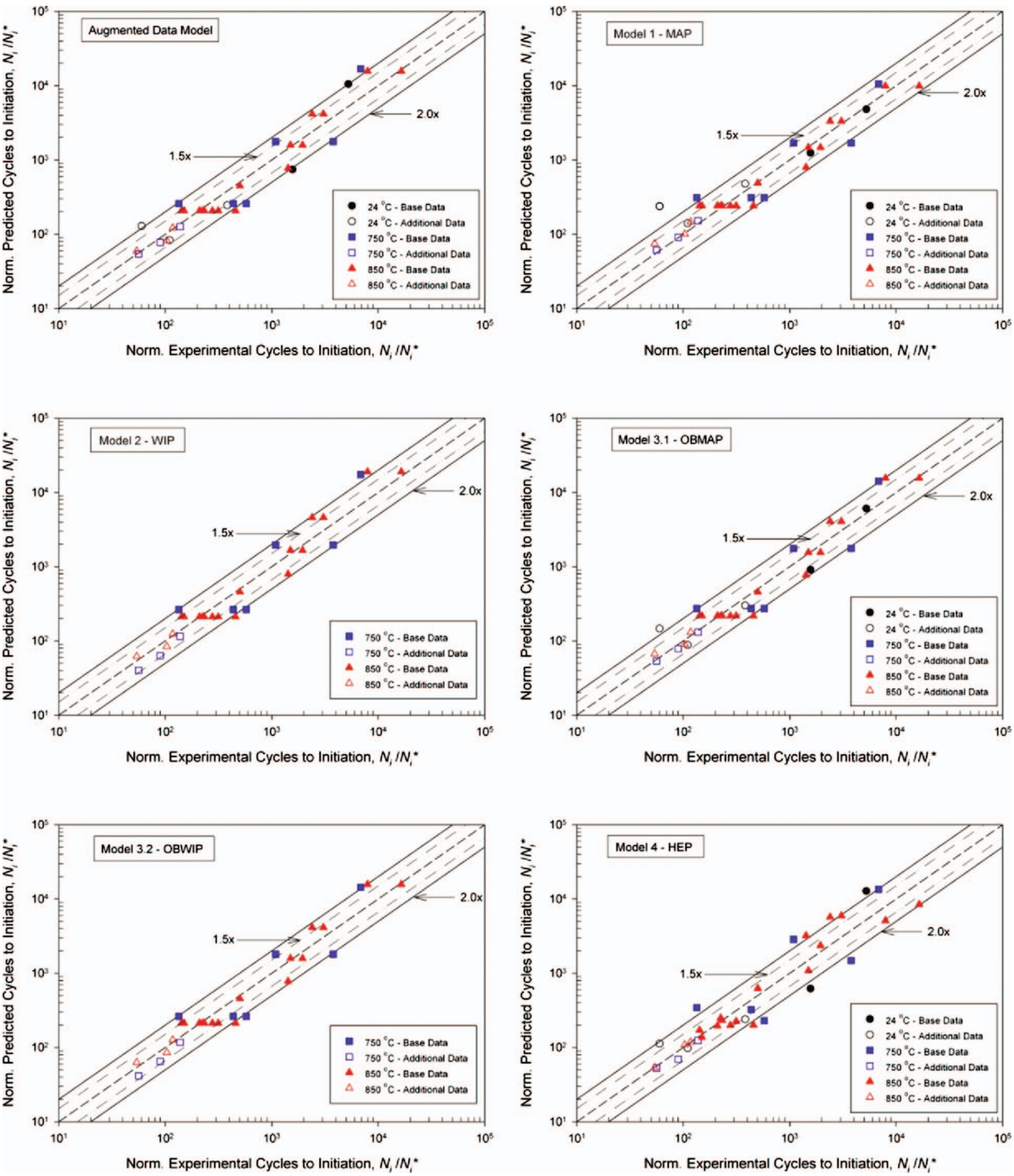

Fig. 10 Comparison of the predicted and experimental life via the various models

7 Conclusions

The intent of this study is to accurately characterize VLCF and high-stress LCF from existing HCF, low-stress LCF, and tensile data. This objective is realized through several novel approaches. Model 1 (MAP) and model 3.1 (OBMAP), although aided by high-stress data, improve upon extrapolation from the augmented data models at 24°C and 750°C. Model 2 (WIP) and model 3.2 (OBWIP) are able to surpass the extrapolation abilities of all other strain-life methods at 850°C. Model 4 (HEP), the energy-life approach, is able to adequately approximate the high-stress augmented data and demonstrate an improved correlation with tensile

Table 7 R^2 correlation of predicted versus experimental life for high-temperature extrapolation

HT R^2	750°C	850°C
Augmented data model	0.9131	0.7658
Base data model	0.6362	0.7617
Model 1—MAP	0.9337	0.4340
Model 2—WIP	0.5579	0.7859
Model 3.1—OBMAP	0.9453	0.7669
Model 3.2—OBWIP	0.6217	0.7881
Model 4—HEP	0.8198	0.9874

data; these observations suggest that energy-factoring methods are most suitable for VLCF behavior. The data used in this study are in accord with results presented in other research; therefore, the products of this project may be exercised with conviction.

In certain instances, the models offered in this study may achieve different results. The inclusion of a modified anchor point significantly improved extrapolation to high-stress regions at 24°C and 750°C; yet, the scaling factors in this research may not relate accordingly to dissimilar data. Conversely, if less scatter is observed in particularly high-plastic localities of data, the employment of either the WIP or OBWIP models may yield superior results at a variety of temperatures. The results of this study provide a strong foundation for further exploration and interpolation of the anchor point modifications. Together, all of the models presented can be functional for different aspects of material testing. The ability to simply provide bounding estimates is exceptionally useful for both material selection purposes and construction of test matrices prior to experimentation. Intermediate temperatures, such as 400°C, were not analyzed, but will be in future research.

As a caution, it should be noted that these methods are not intended for material characterization in the place of ample quantities of valid fatigue data. The techniques employed here demonstrate enhanced prediction capabilities; however, when attempting to forecast fatigue, standard practices should always be performed first.

Acknowledgment

B.R.D. would like to thank David Radonovich, Phillip Gravett, Sachin Shinde, and David Kosich of Siemens Power Generation for their efforts to support this research. A.P.G. is thankful for the support from the Florida Center for Advanced Aero-Propulsion (FCAAP) Technology.

References

[1] Radonovich, D. C., 2007, "Methods of Extrapolating Low Cycle Fatigue Data to High Stress Amplitudes," MS thesis, University of Central Florida, Orlando, FL.
[2] Radonovich, D. C., and Gordon, A. P., 2008, "Methods of Extrapolating Low Cycle Fatigue Data to High Stress Amplitudes," Proceedings of the ASME Turbo Expo 2008: Power for Land, Sea, and Air, Berlin, Germany, Jun. 9–13, pp. 1–10.
[3] Dufailly, J., and Lemaitre, J., 1995, "Modeling Very Low Cycle Fatigue," Int. J. Fatigue, **4**, pp. 153–170.
[4] Morrow, J., and Tuler, F. R., 1965, "Low Cycle Fatigue Evaluation of Inconel 713C and Waspaloy," ASME J. Basic Eng., **87**(2), pp. 275–289.
[5] Manson, S. S., 1965, "Fatigue: A Complex Subject—Some Simple Approximations," Exp. Mech., **5**(7), pp. 193–226.
[6] Manson, S. S., 1968, "A Simple Procedure for Estimating High-Temperature Low-Cycle Fatigue," Exp. Mech., **8**(8), pp. 349–355.
[7] Ong, J. H., 1993, "An Improved Technique for the Prediction of Axial Fatigue Life From Tensile Data," Int. J. Fatigue, **15**(3), pp. 213–219.
[8] Albeirutty, M. H., Alghamdi, A. S., and Najjar, Y. S., 2004, "Heat Transfer Analysis for a Multistage Gas Turbine Using Different Blade-Cooling Schemes," Appl. Therm. Eng., **24**, pp. 563–577.
[9] Balikci, E., 1998, "Microstructure Evolution and Its Influence on Thermal Expansion and Tensile Properties of the Superalloy IN738LC at High Temperatures," Ph.D. thesis, Louisiana State University, Baton Rouge, LA.
[10] Jianting, G., Ranucci, D., Picco, E., and Strocchi, P. M., 1983, "An Investigation on the Creep and Fracture Behavior of Cast Nickel-Base Superalloy IN738LC," Metall. Trans. A, **14**(11), pp. 2329–2335.
[11] Brown, W. F., and Setlak, S. J., 2001, *Aerospace Structural Metals Handbook*, 38th ed., Purdue University, West Lafayette, IN.
[12] Petrenec, M., Obrtlík, J., and Polák, J., 2007, "High Temperature Low Cycle Fatigue of Superalloys Inconel 713LC and Inconel 792-5A," Key Eng. Mater., **348–349**, pp. 101–104.
[13] Hou, N. X., Wen, Z. X., Yu, Q. M., and Yue, Z. F., 2009, "Application of a Combined High and Low Cycle Fatigue Life Model on Life Prediction of SC Blade," Int. J. Fatigue, **31**, pp. 616–619.
[14] ASTM International, 2004, "Standard Practice for Strain-Controlled Fatigue Testing," E606-04, West Conshohocken, PA.
[15] Hyun, J. S., Song, G. W., and Lee, Y. S., 2006, "Thermo-Mechanical Fatigue of the Nickel Base Superalloy IN738LC for Gas Turbine Blades," Key Eng. Mater., **321–323**, pp. 509–512.
[16] Itoh, Y., Saitoh, M., Takaki, K., and Fujiyama, K., 2001, "Effect of High-Temperature Protective Coatings on Fatigue Lives of Nickel-Based Superalloys," Fatigue Fract. Eng. Mater. Struct., **24**(12), pp. 843–854.
[17] Nickel Development Institute, 1985, "Alloy IN738 Technical Data Leaflet," Inco Limited Publication No. 497.
[18] Scarlin, R. B., 1975, "Fatigue Crack Growth in a Cast Ni-Base Alloy," Mater. Sci. Eng., **21**(2), pp. 139–147.
[19] Matsuda, N., Umezawa, S., and Terunuma, F., 1986, "Small Crack Initiation and Growth Behavior of IN738LC at Low Cycle Fatigue and Thermal Fatigue," J. Soc. Mater. Sci. Jpn., **35**, pp. 100–106.
[20] Marchionni, M., Ranucci, D., and Picco, E., 1982, "High-Temperature Low-Cycle Fatigue Behaviour of IN738LC Alloy in Air and in Vacuum," Proceedings of the High Temperature Alloys for Gas Turbines Conference, Liege, Belgium, Oct. 4–6, pp. 791–804.
[21] Day, M. F., and Thomas, G. B., 1985, "Analysis of the Low Cycle Fatigue Behaviour of Two Ni-Cr-Base Alloys," Fatigue Fract. Eng. Mater. Struct., **8**(1), pp. 33–48.
[22] Ondera, H., Ro, Y., Yamagata, T., and Yamazaki, M., 1986, "The Effect of Tensile Strength and Ductility on High-Temperature Low-Cycle Fatigue of Cast Ni-Base Superalloys," Transactions of the National Research Institute for Metals, **28**(2), pp. 112–120.